The Astrophysical Journal, 699:1473–1479, 2009 July 10 doi:10.1088/0004-637X/699/2/1473

X-RAY AND INFRARED OBSERVATIONS OF TWO EXTERNALLY POLLUTED WHITE DWARFS

M. Jura[1], M. P. Muno[2], J. Farihi[3], and B. Zuckerman[1]
[1] Department of Physics and Astronomy and Center for Astrobiology, University of California, Los Angeles, CA 90095-1562, USA; jura@astro.ucla.edu, ben@astro.ucla.edu
[2] Space Radiation Laboratory, California Institute of Technology, Pasadena, CA 90025, USA; mmuno@srl.caltech.edu
[3] Department of Physics and Astronomy, University of Leicester, University Road, Leicester LE1 7RH, UK; jf123@star.le.ac.uk
Received 2009 January 13; accepted 2009 May 8; published 2009 June 23

ABSTRACT

With *XMM-Newton* and the *Spitzer Space Telescope*, we obtain upper bounds to the X-ray fluxes from G29-38 and GD 362, and the 70 μm flux from G29-38. These data provide indirect evidence that G29-38 is accreting from a tidally disrupted asteroid: it is neither accreting large amounts of hydrogen and helium nor is its surrounding dusty disk being replenished from a reservoir of cold grains experiencing Poynting–Robertson drag. The upper bound to the X-ray flux from GD 362 is consistent with the estimated rate of mass accretion required to explain its pollution by elements heavier than helium. GD 362 also possesses 0.01 $M_{\oplus}$ of hydrogen, an anomalously large amount for a white dwarf with a helium-dominated atmosphere. One possibility is that before the current disk was formed, this hydrogen was accreted either from ∼100 Ceres-like asteroids or one large object. An alternative scenario which simultaneously explains all of GD 362's distinctive properties is that we are witnessing the consequences of the tidal destruction of a single parent body that had internal water and was at least as massive as Callisto and probably as massive as Mars.

Key words: planetary systems – white dwarfs

1. INTRODUCTION

At least 1% of single white dwarfs with cooling ages less than 0.5 Gyr are known to display both infrared excess emission and photospheric elements heavier than helium (Farihi et al. 2009). Since primordial heavy atoms gravitationally settle below the atmospheres in these stars, the observed heavy atoms have likely been accreted from their circumstellar disks (Koester 2009). Evidence is strong that these disks are derived from the tidal disruption of an asteroid or minor planet (Jura 2008). If so, then the abundances in the atmospheres of white dwarfs can serve as an indirect but uniquely powerful tool to measure the bulk composition of extrasolar planetary matter (Zuckerman et al. 2007). For example, from the limited data now available, it appears that extrasolar asteroids resemble the inner solar system with values of n(C)/n(Si) or n(C)/n(Fe) at least a factor of 10 below solar (Jura 2006; Farihi et al. 2009).

Models of the infrared excess (Jura et al. 2007a) and measurements of double-peaked calcium triplet emission (Gaensicke et al. 2006, 2007, 2008) both show that white dwarf disks have orbital radii of $\sim 10^{10}$ cm even though these stars previously had radii of $\sim 10^{13}$ cm when they were on the asymptotic giant branch (AGB). The most plausible explanation for the origin of these disks is that an asteroid had its orbit sufficiently perturbed (Debes & Sigurdsson 2002) that it entered the tidal zone of the white dwarf and was shredded (Jura 2003). Even with this scenario for disk formation, we have very limited constraints on the disk masses, lifetimes, and compositions such as the relative amounts of gas, rock, and ice. Here, we present new X-ray and infrared data which enable an improved measure of the evolution of the disks orbiting two accreting white dwarfs and thus enhance their use as probes of extrasolar planetary systems.

G29-38 and GD 362 were the first and second single white dwarfs, respectively, found to have an infrared excess (Zuckerman & Becklin 1987; Becklin et al. 2005; Kilic et al. 2005). As with other DA (hydrogen-dominated) white dwarfs, only a few heavy elements have been identified in the atmosphere of G29-38 (Zuckerman et al. 2003). However, GD 362's atmosphere is helium-dominated and this star displays a rich spectrum (Gianninas et al. 2004) with 17 identified elements (Zuckerman et al. 2007). With silicon as a standard, GD 362 is enhanced in refractories such as calcium and titanium and deficient in volatiles such as sodium and carbon.

Reach et al. (2009) present two models to account for G29-38's 5–40 μm infrared spectrum; their optically thin model requires water-ice while the optically thick model does not. It is possible, but unproven, that white dwarf disks possess hydrogen as well as dust. With X-ray observations of G29-38, we can assess the amount of gas this hydrogen-dominated star accretes.

The shape of its 10 μm silicate feature indicates that G29-38 is orbited by dust from a disrupted comet or asteroid rather than from the interstellar medium (Reach et al. 2005, 2009). However, these data, by themselves, do not allow us to decide whether the dust originates near the star from a tidally disrupted asteroid (Jura 2003) or, instead, arises in a cold outer reservoir and then drifts inward to replenish the observed warm disk, as occurs around some main-sequence stars (Chen et al. 2006). Here, we report 70 μm observations of G29-38 which constrain the rate of inward drift of dust grains from an outer cold reservoir onto the warm disk.

Two recent studies of white dwarfs with helium-dominated photospheres propose that much of their atmospheric hydrogen arises from accretion of interstellar matter (Dufour et al. 2007; Voss et al. 2007). GD 362 has an anomalously high hydrogen content, and we consider if this could have resulted from accretion of an object or objects with a substantial amount of interior water.

In Section 2, our X-ray observation shows how these data can be used to constrain the gas accretion rates. In Section 3, we report our 70 μm data and describe how they can be used to constrain the rate of dust infall from a cold reservoir. In Section 4, we describe observations and constraints on the hydrogen in GD 362's photosphere. In Section 5, we discuss our results and in Section 6 we present our conclusions.

Table 1
X-Ray Counts

Star	Band (kev)	pn On	pn Off	pn Net	MOS On	MOS Off	MOS Net	Flux 10^{-15} erg cm^{-2} s^{-1}
G29-38	0.3–2.0	17	9.3	<15	7	6.3	<6	<1
	0.3–10.0	23	15.2	<16	12	11.5	<7	<2
GD362	0.3–2.0	14	17.0	<6	8	10.3	<5	<0.7
	0.3–10.0	31	33.2	<9	19	21.3	<7	<2

Note. Upper limits are 90% confidence.

Table 2
Stellar Properties

Star	D (pc)	M_* ($M_\odot$)	R_* (10^8 cm)	$\dot{M}_X$[a] (10^9 g s^{-1})	$t_{\rm cool}$[b] (Gyr)
G29–38	14	0.61	8.5	<2	0.4
GD 362	50	0.71	7.4	<20	0.7–0.8

Notes.
[a] See Equation (1).
[b] White dwarf cooling age.

2. X-RAY RESULTS

2.1. Data

Using *XMM-Newton*, G29-38 was observed for 23 ks starting on 2005 November 28 at 21:04:33 UTC, and GD 362 was observed for 5 ks starting on 2006 September 4 at 02:06:23 UTC and for 14 ks starting on 2006 September 8 at 01:50:55 UTC. We analyzed the data taken with the European Photon Imaging Camera (EPIC) using standard procedures.[4] We processed the observation data files using the tools epchain and emchain from the Science Analysis Software version 7.0. The events were filtered to remove events near the edges of the detector chips and bad pixels, and to reject events that were likely to be cosmic rays. We then examined the data for solar flares in the particle background, during which the detector counts from each array were two standard deviations above the mean count rate. Flares lasting ≈5 ks were found in all detectors during the observation of G29-38, and one lasting 1 ks was found in the 2006 September 4 observation of GD 362. We ignored the data taken during the flaring intervals, leaving exposures of G29-38 totaling 17.1 ks in the pn detector (Struder et al. 2001) and 18.5 ks in each MOS detector (Turner et al. 2001), and of GD 362 totaling 18.1 ks in the pn detector and 20.7 ks in each MOS detector.

We found that neither source was detected in any of the exposures. We computed upper limits to the net counts received by comparing the number of photons received within a 15″ radius circle centered on the source to the number received within a 1′ radius circle placed on blank sky 1.′5 away from of each source, using the algorithm described in Kraft et al. (1991). The counts in the on-source region, the off-source region, and the derived net counts are listed in Table 1.

G29–38 is located only 15″ from an unidentified X-ray point source ($\alpha, \delta = 23^{\rm h}28^{\rm m}46\overset{\rm s}{.}7, +05^\circ14'50''$) with 30 ± 10 counts in both the pn and the combined MOS detectors, which slightly complicated our derivation of an upper limit. As can be seen in Table 1, there is marginal evidence for an excess in the pn detector, but no such evidence in the MOS detector. However, the pn detector has much larger pixels than the MOS detector (4.″1 versus 1.″1), so we conclude that these excess counts are an artifact of uncertainties in the shape of the point-spread function. We converted the count rates to fluxes using the Portable Multi-Mission Simulator,[5] and list them in Table 1. For the 0.3–2.0 keV band, we assumed that the emission could be described by a 0.5 keV plasma. For the 0.3–10 keV band, we assumed that it would originate from 5 keV thermal bremsstrahlung. Interstellar absorption is negligible toward both sources.

[4] http://xmm.vilspa.esa.int/external/xmm_user_support/documentation/sas_usg/USG
[5] http://heasarc.gsfc.nasa.gov/Tools/w3pimms.html

2.2. Implications

Accretion onto white dwarfs can produce X-ray emission, and we use our observational upper limits to constrain the mass flux onto the observed stars. Szkody et al. (2004) and Schmidt et al. (2007) have investigated X-ray emission from white dwarfs with accretion rates as low as 4 × 10^{12} g s^{-1}, and we follow their analysis. We thus assume that the accretion flows onto G29-38 and GD 362 are in the "bombardment regime" described by Kuijpers & Pringle (1982). In such an environment, a gas layer with a temperature near 10^7 K is formed, and this hot gas freely radiates away the accretion energy. Consequently, because half of the emitted photons are radiated into the photosphere and other photons are emitted at wavelengths outside of the *XMM-Newton* MOS bandpass, we make the very simple approximation for the X-ray luminosity, L_X, that (Patterson & Raymond 1985)

$$L_X \approx \frac{1}{4}\frac{G\dot{M}_X M_*}{R_*} \quad (1)$$

Here, $\dot{M}_X$ is the mass accretion rate inferred from X-rays, and M_* and R_* are the mass and radius of the white dwarf, respectively.

We list in Table 2, our adopted values of the stellar masses, radii and distances (Kilic et al. 2008a, Reach et al. 2009; Farihi et al. 2009) as well as the inferred value of $\dot{M}_X$ as derived from Equation (1) and the X-ray fluxes listed in Table 1. Our X-ray data for G29-38 show that the upper limit to the mass accretion rate of 2 × 10^9 g s^{-1} is consistent with the heavy element accretion rate of 5 × 10^8 g s^{-1} required to explain this star's composition (Farihi et al. 2009) and inconsistent with the accretion rate of 5 × 10^{10} g s^{-1} expected for hydrogen-rich interstellar matter (Koester & Wilken 2006). Our result also is consistent with the estimate by Reach et al. (2009) that the mass in water-ice is 1/4 the mass in olivine in the material orbiting G29-38. The settling time for heavy elements in G29-38's hydrogen-dominated atmosphere is less than one year (Koester 2009), and therefore a steady state model is appropriate. However, the characteristic heavy element settling time in GD 362's atmosphere is ∼10^5 yr (Table 3 and Koester 2009). In Section 4, we present time-dependent models for the accretion that are consistent with the upper bound to the X-ray luminosity. The X-ray limit is also consistent with the sum of the accretion rates derived from Equation (10) in Section 4.2 and listed in Table 3.

3. INFRARED RESULTS

3.1. Data

Previously, G29-38 has been observed only at $\lambda < 40$ μm (Reach et al. 2009). Here we report observations of G29-38 at

Table 3
Heavy Elements in GD 362's Convective Envelope

Element	$M_{\rm mix}(Z)$[a] (10^{21} g)	$t_{\rm set}$[b] (10^5 yr)	$\dot{M}_*(Z,t)$[c] (10^9 g s^{-1})
O	<11	1.13	<3.1
Mg	$2.4^{+1.9}_{-1.0}$	0.944	$0.81^{+0.64}_{-0.34}$
Al	$1.0^{+0.65}_{-0.34}$	0.857	$0.37^{+0.24}_{-0.12}$
Si	$3.9^{+3.9}_{-1.9}$	0.795	$1.6^{+1.5}_{-0.80}$
Ca	$2.2^{+0.60}_{-0.40}$	0.607	$1.2^{+0.26}_{-0.26}$
Fe	$12^{+3.0}_{-2.4}$	0.467	$8.2^{+2.0}_{-1.7}$
Ni	$0.48^{+0.20}_{-0.14}$	0.445	$0.34^{+0.15}_{-0.10}$
Total[d]	33.0		15.6[e]

Notes.
[a] Current value from the relative abundances in Zuckerman et al. (2007) and the assumption that $M_{\rm mix}(H) = 7.0 \times 10^{24}$ g (Koester 2009).
[b] From Koester (2009).
[c] Evaluated from Equation (16).
[d] Assuming that the true oxygen value equals the upper limit.
[e] Consistent with the upper limit derived from the X-ray data of 2×10^{10} g s^{-1}.

70 μm that were executed on 2008 July 28 with the Multiband Imaging Photometer for *Spitzer* (MIPS; Rieke et al. 2004; Werner et al. 2004). Using the default camera settings and small field of view, the white dwarf was imaged over 40 cycles of the MIPS dither using 10 s exposures and the default dither pattern, for a total integration time of 4.4 ks.

Owing to the expected target faintness, the data reduction was performed on the median-filtered basic calibrated data frames, which produced a higher quality mosaic than the non-filtered frames, in this instance. The mosaics were created using MOPEX,[6] and photometry was performed on the final image produced from the filtered frames. There was no apparent source of flux at the expected location of the white dwarf, and this was verified by aperture photometry executed with a radial 16″ (4 pixel) aperture and a sky annulus between 18″ and 39″ from G29-38. The sky noise per pixel was measured within the 4 pixel aperture radius, multiplied by the square root of the number of aperture pixels, and multiplied by the average of the 60 K and 10 K aperture corrections (2.185) found in the MIPS Data Handbook version 3.3.1 (Spitzer Science Center 2007). The resulting 3σ upper limit is 1.32 mJy.

3.2. Implications

We use the upper limit to the 70 μm flux from G29-38 to place an upper limit to the rate of dust infall from a cold reservoir, $\dot{M}_{\rm dust}$. If the particles orbit at some initial radius, $D_{\rm init}$, and subsequently drift inward because of Poynting–Robertson drag until they reach a final radius, $D_{\rm final}$, then the flux, F_ν at frequency ν is (Jura et al. 2007a)

$$F_\nu \approx \left[\frac{1}{2}\ln\left(\frac{D_{\rm init}}{D_{\rm final}}\right)\frac{\dot{M}_{\rm dust}\,c^2}{\nu}\right]/(4\pi\,D^2), \qquad (2)$$

where D is the distance from the Earth to the white dwarf. We assume that the reservoir lies at 5 AU where the parent bodies might have a chance of surviving the star's AGB evolution (Jura 2008) and that the grains drift inward until they reach the outer boundary of the circumstellar disk near 10^{10} cm (Jura 2003; Reach et al. 2005, 2009). Therefore, we adopt $D_{\rm init}/D_{\rm final} \approx 10^4$, although our results are insensitive to this ratio which only enters logarithmically into the estimate for $\dot{M}_{\rm dust}$. With $F_\nu(70\ \mu{\rm m}) \leqslant 1.3$ mJy, we find that $\dot{M}_{\rm dust} \leqslant 10^6$ g s^{-1}, a factor of 500 less than the current heavy element accretion rate. We conclude the disk is not being replenished under the action of Poynting–Robertson drag from a reservoir of cold dust. A plausible alternative is that the disk is derived from a tidally disrupted asteroid (Jura 2003).

4. GD 362

4.1. Hydrogen to Helium Ratio

Zuckerman et al. (2007) found that GD 362's atmosphere has an appreciable mixture of hydrogen and helium. Because accurate models for the outer layers of white dwarfs with such a mixed composition were not available, they could only report the abundance ratio of hydrogen to helium but not the total amount of hydrogen. Subsequently, Koester (2009) computed a detailed model for GD 362's outer envelope, and, using the observations of Zuckerman et al. (2007), found that there is 7.0 $\times$ 10^{24} g of the hydrogen in the star's mixing layer. We now consider possible explanations.

The relative amount of hydrogen and helium in the atmospheres of helium-dominated white dwarfs is not fully understood (Tremblay & Bergeron 2008; E. Y. Chen & B. Hansen 2009, in preparation. Regardless, it appears that GD 362 is unusual. Zuckerman et al. (2007) measured n(He)/n(H) = 14 in GD 362's photosphere, and there are two possible scenarios to explain this measurement. First, the star may have been a hydrogen-dominated white dwarf until it cooled to an effective temperature less than 11,000 K. At this temperature, the mass of the convective envelope increased, and it is possible that some interior helium was dredged up to the surface (Tremblay & Bergeron 2008). However, even if this scenario correctly describes GD 362's history, the star still may be unusual. Bergeron et al. (1990) analyzed 37 DA white dwarfs and with the assumption that all the stars have log g = 8.0, they found that most have n(He)/n(H) < 1, but deduced that G1-7 and G67-23 have n(He)/n(H) $\approx$ 20, near the ratio determined for GD 362. However, these two abundance ratios are questionable. Helium absorption lines in G1-7 and G67-23 are not directly measured; instead helium abundances are inferred from the hydrogen line profiles. Broadening caused by an increased helium abundance and broadening stemming from an increased surface gravity are degenerate (Zuckerman et al. 2003), and the assumed value of log g for these two stars are probably too low. For G1-7, Liebert et al. (2005) derived log$g$ = 8.83, while for G67-23, Zuckerman et al. (2003) and Holberg et al. (2008a) derived log g = 8.5 and 8.8, respectively. The trigonometric parallax for G67-23 supports the high-gravity model (Holberg et al. 2008b). Therefore, the photospheric value of n(He)/n(H) in GD 362 may be uniquely high for a DA white dwarf.

A second possibility is that GD 362 has been evolving continuously as a star with a helium-dominated atmosphere. In Figure 1, we display the hydrogen masses in the convective zones of helium-dominated white dwarfs from Voss et al. (2007) and Dufour et al. (2007) for stars in the temperature range 8000 K $\leqslant T \leqslant$ 20,000 K. Dufour et al. (2007) report values of n(H)/n(He), and we use these ratios along with the total mass in the convective zone for helium-dominated white dwarfs from Koester (2009), a value which typically is near 2 $\times$ 10^{28} g, to determine the mass of hydrogen in the white dwarf's atmosphere. For reference, we also plot the amount of hydrogen in Ceres and Callisto by assuming water contents

[6] http://ssc.spitzer.caltech.edu/postbcd/mopex.html

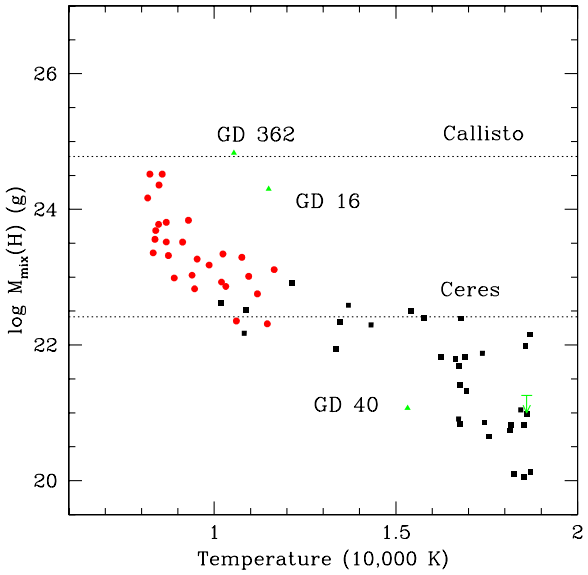

Figure 1. Mixing envelope mass of hydrogen ($M_{\rm mix}(H)$) for helium-dominated white dwarfs. Black squares are from Voss et al. (2007), red circles are from Dufour et al. (2007), and green triangles are white dwarfs with an infrared excess. The green upper limit refers to Ton 345 which is a heavy-element polluted helium-dominated white dwarf without detected hydrogen (Gaensicke et al. 2008) and with an infrared excess (C. Melis et al. 2009, in preparation). The atmospheric mass of hydrogen for GD 16 is taken from the observed hydrogen abundance (Koester et al. 2005) and the calculation by Koester (2009, private communication) that the total mass in the star's convective envelope is 6.3×10^{27} g. The hydrogen masses for GD 362 and GD 40 are from Koester (2009) and Voss et al. (2007), respectively. The dotted lines show the estimated hydrogen masses in Callisto and Ceres (see Section 5).

of 25% by mass and 50% by mass, respectively (Michalak 2000; McCord & Sotin 2005; Thomas et al. 2005; Canup & Ward 2002), and, as standard in these models, by assuming that the hydrogen is largely contained within H_2O. We see from Figure 1 that the total mass of hydrogen in GD 362's convective envelope appears anomalously large. GD 16 is another helium-dominated star with a distinctively large amount of hydrogen and an infrared excess. Both Voss et al. (2007) and Dufour et al. (2007) attribute much of the hydrogen in the atmospheres of white dwarfs with helium-dominated atmospheres to accretion from the interstellar medium. Because GD 362 has both an infrared excess and a substantial atmospheric pollution of heavy atoms, we consider models where its hydrogen is derived from a tidally disrupted parent body. During the star's red giant evolution before reaching the AGB and becoming a white dwarf, it sublimated surface water-ice from any orbiting parent body within at least 40 AU (Jura 2004). We imagine that the parent body or bodies that have been accreted by GD 362 had internal water to account for the atmospheric hydrogen as, for example, in models of Callisto (Canup & Ward 2002).

4.2. Schematic Model

We model GD 362's atmospheric abundances of hydrogen and heavy elements, as well as the upper limit to the current accretion rate derived in Section 2.2. We assume that a parent body of mass, $M_{\rm par}$, has its orbit perturbed so that it is tidally disrupted by the white dwarf (Debes & Sigurdsson 2002; Jura 2003), and this defines the starting time, $t = 0$, of the accretion event. The debris is rapidly reduced by mutual collisions to small dust particles, some at least as small as 1 μm in radius to account for the strong silicate emission (Jura et al. 2007b), and the material forms a disk. Material in this disk then accretes onto the star with a characteristic timescale $t_{\rm disk}$ that is determined by viscous dissipation. We write for the mass of the disk, $M_{\rm disk}(t)$, that

$$M_{\rm disk}(t) \;=\; M_{\rm par}\, e^{-t/t_{\rm disk}}. \tag{3}$$

The accretion rate onto the star, $\dot{M}_*$, equals $-\dot{M}_{\rm disk}$ or

$$\dot{M}_*(t) \;=\; \frac{M_{\rm par}}{t_{\rm disk}}\, e^{-t/t_{\rm disk}}. \tag{4}$$

Because hydrogen rises to the top, the total mass of hydrogen in GD 362 is the amount in the mixing layer, $M_{\rm mix}(H, t)$, and

$$M_{\rm mix}(H,t) = \int_0^t \dot{M}_*(H,t')\,dt' \;=\; M_{\rm par}(H)\,(1-e^{-t/t_{\rm disk}}). \tag{5}$$

In Section 4.3, we use observational constraints to derive the composition of the parent body as a function of t and $t_{\rm disk}$. Thus,

$$M_{\rm par}(H) \;=\; \frac{M_{\rm mix}(H,t)}{1\;-\;e^{-t/t_{\rm disk}}}. \tag{6}$$

The total mass of heavy element Z in the mixing layer of the star, $M_{\rm mix}(Z, t)$, is governed by both the gain from accretion and the loss from settling which are described by Dupuis et al. (1993) as

$$\frac{dM_{\rm mix}(Z,t)}{dt} \;=\; \dot{M}_*(Z,t) \;-\; \frac{M_{\rm mix}(Z,t)}{t_{\rm set}(Z)}. \tag{7}$$

In Equation (7), $t_{\rm set}(Z)$ denotes the time that element Z takes to settle out of the surface mixing layer. With the boundary condition that $M_{\rm mix}(Z, t) = 0$ at $t = 0$, then

$$M_{\rm mix}(Z,t) \;=\; \frac{M_{\rm par}(Z)\,t_{\rm set}(Z)}{t_{\rm disk}\;-\;t_{\rm set}(Z)}\,(e^{-t/t_{\rm disk}} \;-\; e^{-t/t_{\rm set}(Z)}). \tag{8}$$

We define a time-related parameter, $\tau(Z)$, which can be either positive or negative, for each element

$$\tau(Z) \;=\; \frac{t_{\rm disk}\,t_{\rm set}(Z)}{t_{\rm disk}\;-\;t_{\rm set}(Z)}. \tag{9}$$

With Equations (4) and (9), Equation (8) becomes

$$M_{\rm mix}(Z,t) \;=\; \dot{M}_*(Z,t)\,\tau(Z)\,(1-e^{-t/\tau(Z)}). \tag{10}$$

In Section 4.3, we infer the composition of the parent body from $M_{\rm mix}(Z, t)$. Thus, from Equations (8)–(10)

$$M_{\rm par}(Z) \;=\; \frac{M_{\rm mix}(Z,t)\,t_{\rm disk}\,e^{t/t_{\rm disk}}}{\tau(Z)(1\;-\;e^{-t/\tau(Z)})}. \tag{11}$$

To compute the mass of oxygen in the parent body, we assume this element is carried in water and oxides. Thus,

$$M_{\rm par}(O) \;=\; \frac{m_O}{2\,m_H}\,M_{\rm par}(H) + \sum \frac{n(O)\,m_O}{n(Z)\,m_Z}\,M_{\rm par}(Z), \tag{12}$$

where the mean atomic weight of each element is denoted by m_Z and the $n's$ denote the number of atoms in the oxide $Z_{n(Z)}O_{n(O)}$.

To illustrate our model, we consider various limiting cases which are seen in detail in Section 4.3. If $t \ll t_{\rm set}(Z)$ and $t \ll t_{\rm disk}$, then Equation (11) can be approximated as

$$M_{\rm par}(Z) \approx M_{\rm mix}(Z,t)\,\frac{t_{\rm disk}}{t}. \tag{13}$$

Thus, at early times, a large parent body mass is required to reproduce the observed pollution because only a small fraction of its initial mass has been accreted. In the case with $t > t_{\rm disk}$ and $t_{\rm disk} \gg t_{\rm set}$, then Equation (11) becomes

$$M_{\rm par}(Z) \approx M_{\rm mix}(Z,t)\,\frac{t_{\rm disk}}{t_{\rm set}(Z)}\,e^{t/t_{\rm disk}}. \quad (14)$$

At long times a large parent body mass is required because most of its mass has accreted and settled below the mixing layer. At intermediate times, $M_{\rm par}(Z)$ achieves a minimum. In the circumstance where $t_{\rm disk}$ is only slightly larger than $t_{\rm set}(Z)$, then as seen in Equation (9), $\tau(Z)$ becomes relatively large compared to $t_{\rm set}$. Thus, when $t \gg \tau(Z)$, by Equation (10), $M_{\rm mix}(Z,t)$ is enhanced over cases where $\tau(Z) \approx t_{\rm set}(Z)$.

In Section 4.3, we compare the sum of the accretion rates for each element, $\dot{M}_*(Z,t)$, as derived from the optical data, with the upper bound from the X-ray data. When $t \gg \tau(Z)$ and $\tau > 0$, then from Equation (10)

$$\dot{M}_*(Z,t) \approx \frac{M_{\rm mix}(Z,t)}{\tau(Z)}. \quad (15)$$

In the limit that $t_{\rm disk} \gg t_{\rm set}$, Equation (15) becomes

$$\dot{M}_*(Z,t) \approx \frac{M_{\rm mix}(Z,t)}{t_{\rm set}(Z)}. \quad (16)$$

4.3. Application to GD 362

If GD 362 has always had a helium-dominated atmosphere, two sorts of models may explain its atmospheric hydrogen. One possibility is that the hydrogen was accreted prior to the era when the currently orbiting disk was formed. This earlier accretion could have been from either one large parent body or a swarm of asteroids. Alternatively, one event may account for all of GD 362's distinctive properties, and using the formalism of Section 4.2, we now describe such a model.

The observational constraints to be matched are the observed atmospheric abundances of hydrogen and detected elements heavier than oxygen contributing at least 1% of the accreted mass, and the upper limits to the mass accretion rate and the atmospheric oxygen abundance. As in the Earth (Palme & O'Neill 2004), we assume that within the parent body, aluminum, magnesium, silicon, and calcium are contained in the oxides MgO, Al_2O_3, SiO_2, and CaO while iron and nickel are largely metallic. Although oxygen is not detected in GD 362's photosphere, our expectation of a parent body composed substantially of oxides is consistent with the fit of GD 362's 10 μm emission feature by grains with an olivine stoichiometry (Jura et al. 2007b). As in the Earth's interior, we assume that hydrogen is largely contained within H_2O (Wood et al. 1996). Therefore, the 7.0×10^{24} g of hydrogen in GD 362's implies the parent body must have possessed at least 5.6×10^{25} g of oxygen. Table 3 provides details.

A major uncertainty is the disk lifetime, $t_{\rm disk}$. Jura (2008) proposed that $t_{\rm disk} = 1.5 \times 10^5$ yr by estimating the viscosity in a disk composed mostly of dust with some additional gas. Kilic et al. (2008b) suggested a value of $t_{\rm disk}$ to be $\sim 10^5$ yr since HS 2253+803, a heavily polluted white dwarf with a helium-dominated atmosphere, does not have an infrared excess. Von Hippel et al. (2007) and Farihi et al. (2008) argued that disks composed purely of dust may survive over 10^9 yr. All these estimates are very uncertain and $t_{\rm disk}$ may vary from one disk to another. We therefore consider models where $t_{\rm disk}$ ranges from 2×10^5 yr to 10^8 yr. We truncate all the calculations at $t > 30\ t_{\rm disk}$ because, by this time, the material has largely dissipated. We do not display results from models with $t_{\rm disk}$ as low as 10^5 yr since such models do not match the data because, according to Equation (9), $\tau(O)$ is negative and the models behave qualitatively differently from the ones we show.

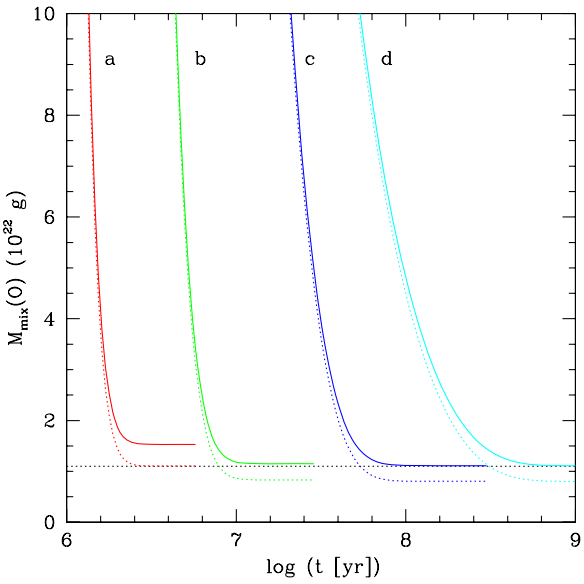

Figure 2. Predicted mixing envelope mass of oxygen ($M_{\rm mix}(O)$) in GD 362 as a function of time. The red (model a), green (model b), blue (model c), and cyan (model d) lines refer to values of $t_{\rm disk}$ of 2×10^5, 10^6, 10^7, and 10^8 yr, respectively. The solid and dotted lines refer to models where the silicon mass in the mixing zone is the nominal value and the lower bound, respectively, as listed in Table 3. The dotted horizontal black line denotes the observational upper limit from Table 3.

To match the observational constraints, we follow the schematic model in Section 4.2. For any given value of t and $t_{\rm disk}$, we first compute $M_{\rm par}$ from Equations (6), (11), and (12). We then compute current values of $\dot{M}_*$ from Equation (4) and $M_{\rm mix}$(O) from Equation (8). The results are displayed in Figures 2–4.

Figure 2 shows the predicted mass of oxygen in the mixing layer. Because silicon's abundance is more uncertain than that of most other heavy elements and because it is the most important carrier of oxygen among the heavy elements, we explicitly show models for both the nominal and low values of $M_{\rm mix}$(Si) given in Table 3. In all models, the expected amount of oxygen initially is much greater than the observed upper limit because the parent body must be largely water to explain the observed ratio of hydrogen to heavy elements. However, at later times, most of the heavy elements accreted from the parent body have settled below the mixing layer, and $M_{\rm mix}$(O) asymptotically nears or falls below the observational upper limit.

Figure 3 shows the model predictions for the total accretion rate as a function of time. Initially, the models all predict a high accretion rate because, as illustrated by Equation (13), a massive parent body is required. Ultimately, at long times, in all models, $\dot{M}_*$ approaches an asymptotic value defined by Equation (15) or (16), and as listed in Table 3, is less than the upper limit derived from the X-ray data.

Figure 4 shows the inferred mass of the parent body for different models. We also display on each curve the times when the model first achieves agreement with the limits on the total accretion rate and the mass of oxygen in the mixing

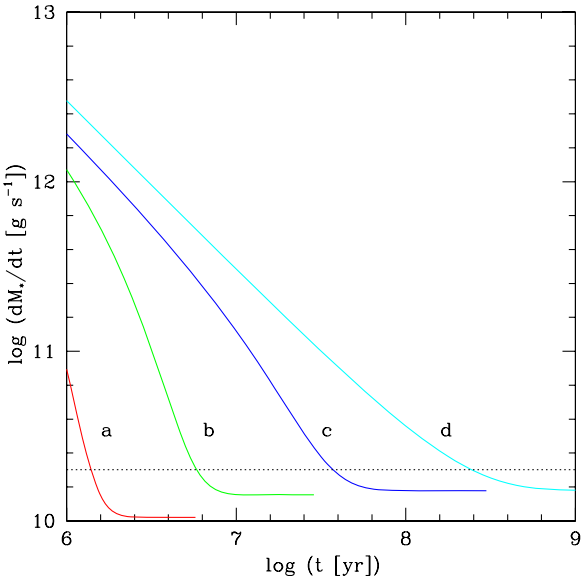

Figure 3. Inferred mass accretion rates ($\dot{M}_*$). The different colored lines are defined as in Figure 2. Only solid curves are shown because the differences in $\dot{M}_*$ between the models with nominal and low silicon mass in the mixing zone are not significant. The dashed horizontal line denotes the upper limit from our X-ray data.

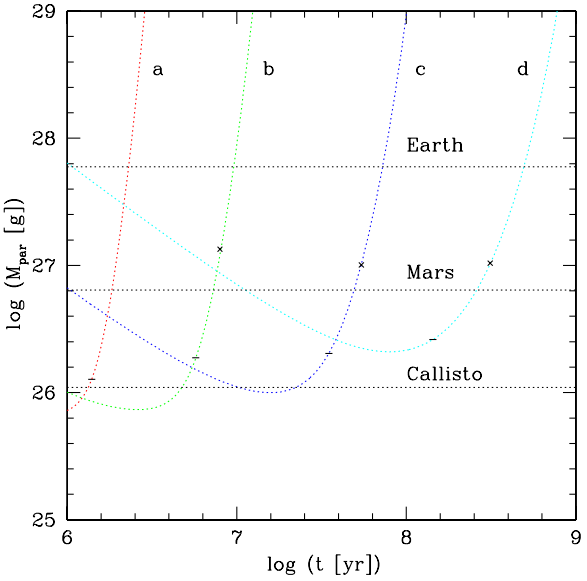

Figure 4. Inferred total mass of the parent body ($M_{\rm par}$) required to fit the observational constraints. Each colored line as defined in Figure 2 is marked by a solid black dash at the first time when the accretion rate falls below the inferred upper limit of 2×10^{10} g s^{-1} (as shown in Figure 3) and a black cross at the first time when the oxgyen mass in the mixing zone falls below its upper limit of 1.1×10^{22} g (as shown in Figure 2). These results are displayed for the case using the lower bound of the silicon mass in the mixing zone, the dotted curves in Figure 2.

zone. Agreement is achieved with the data only when the parent body mass is greater than that of both Callisto and Mars. The minimum mass of the parent body required to satisfy the data is insensitive to the disk lifetime for $t_{\rm disk} > 10^6$ yr.

We now estimate heavy element composition in the parent body of the material accreted onto GD 362. Since only models with $t \gg t_{\rm disk}$ fit the data, we derive $M_{\rm par}(Z)$ from Equation (16) and the parameters listed in Table 3 with the additional assumption that oxygen accretes at its derived upper limit. We show in Table 4 the results and compare with values for the bulk Earth.

Table 4
Element Fractional Composition by Mass in GD 362's Polluting Parent Body

Element	Parent Body[a]	Bulk Earth[b]
O	0.20	0.32
Mg	0.052	0.16
Al	0.024	0.015
Si	0.10	0.17
Ca	0.078	0.016
Fe	0.53	0.28
Ni	0.022	0.016

Notes.
[a] From the accretion rates in Table 3 and ignoring minor constituents. We assume oxygen accretes at its derived upper limit.
[b] From Allegre et al. (1995). The total fraction is less than 1.00 because we omit minor constituents.

The inferred 6.3×10^{25} g of internal water in the model GD 362 parent body is much greater than the (2–8) $\times 10^{24}$ g of internal water in the Earth (Wood et al. 1996).

5. DISCUSSION

How can we better understand the parent body or bodies accreted onto GD 362? Since the mass of the main-sequence progenitor to GD 362 was $\sim 3\ M_\odot$ (Kilic et al. 2008b), the thermal history of its planet-forming nebula and resulting planetesimals and planets likely were different from that of the solar nebula. This might account for the relatively high abundance of calcium in GD 362's polluted photosphere. In any case our unified model for GD 362's pollution with the assumption that magnesium, aluminum, silicon, and calcium are contained within oxides could be falsified with better measurement of the star's elemental abundances, particularly oxygen and silicon. Also, relative to the Sun, the Earth is deficient in volatiles like chlorine, sulfur, and phosphorus by factors of $\sim$10 to $\sim$100 (Palme & O'Neill 2004). Measurements of the abundances of these volatile elements could help clarify the origin and evolution of the parent body responsible for polluting GD 362.

It is possible that the atmospheric hydrogen in GD 362 was derived from the accretion of many small asteroids rather than one single large object. The indicated minimum mass of the accreted material onto GD 362 of $\sim 10^{26}$ g is much larger than the total mass of 2×10^{24} g of the solar system's asteroid belt (Binzel et al. 2000). However, an asteroid belt orbiting the A3V star ζ Lep could be as massive as 4×10^{26} g (Chen & Jura 2001) and such a system could supply the required mass.

There exists evidence for the destruction of massive rocky bodies in extrasolar planetary systems. The main-sequence stars BD +20 307 and HD 23514 have circumstellar dust (Song et al. 2005; Rhee et al. 2008) that likely resulted from collisions of parent bodies of $\sim 10^{26}$ g (Rhee et al. 2008). Ashwell et al. (2005) have proposed that the main-sequence F-type star J37 in the open cluster NGC 6633 has accreted approximately 10^{26} g of material from a disrupted planet. A plausible model for the formation of the Moon is that a Mars-mass planetesimal collided with Earth when the solar system had an age of $\sim$ 25–30 Myr (Canup 2004).

After a planetary system's orbits have been drastically rearranged during the AGB phase mass loss, plausibly, there could be a late perturbation of a Mars-mass planet. If the disk persists for $\sim 10^8$ yr, even very rare events might be salient. The scenario that the disk orbiting GD 362 is the result of the tidal destruction

of a Mars-mass planet is quite different from the suggestion by Reach et al. (2009) that the disk orbiting G29-38 might be debris from the core of a Jovian-mass planet that was engulfed during the AGB phase of the star's evolution. The amount of hydrogen in GD 362's mixing layer is a factor of $\sim 10^5$ less than the mass of Jupiter. Therefore there must have been very efficient but fine-tuned removal of the bulk of a Jovian planet while retaining the rocky core if such a model is to explain GD 362's pollution.

We have raised the possibility that GD 362 has accreted from a parent body with a mass at least as large as 10^{26} g. If a tidally disrupted disk was formed and the dissipation time was as short as 10^5 yr (Jura 2008; Kilic et al. 2008b), then the accretion rate of 3×10^{11} g s^{-1} produced an X-ray luminosity of $\sim 5 \times 10^{27}$ erg s^{-1}. Single white dwarfs typically have X-ray luminosities less than 10^{28} erg s^{-1} (O'Dwyer et al. 2003), but there might be rare exceptions that could be diagnostic of accretion of a large parent body.

6. CONCLUSIONS

Our new X-ray and infrared data are consistent with the scenario that GD 362 and G29-38 are polluted by accretion of material from their circumstellar disks. GD 362 also has an anomalously large mass of hydrogen. One possibility is that before the current disk was formed, GD 362 was bombarded either by a swarm of Ceres-mass asteroids or by a single large object. An alternative model to explain simultaneously all of this star's distinctive properties is that we are witnessing the consequences of the tidal destruction of a single parent body at least as massive as Callisto and probably as massive as Mars.

This work has been partly supported by NASA and the NSF. We thank the referee, F. Mullally, for a careful reading of the manuscript and for asking helpful questions.

REFERENCES

Allegre, C. J., Poirier, J.-P., Humler, E., & Hofmann, A. W. 1995, Earth Planetary Sci. Letters, 134, 515
Ashwell, J. F., Jeffries, R. D., Smalley, B., Deliyannis, C. P., Steinhauer, A., & King, J. R. 2005, MNRAS, 363, L81
Becklin, E. E., Farihi, J., Jura, M., Song, I., Weinberger, A. J., & Zuckerman, B. 2005, ApJ, 632, L119
Bergeron, P., Wesemael, F., Fontaine, G., & Liebert, J. 1990, ApJ, 351, L21
Binzel, R. P., Hanner, M. S., & Steel, D. I. 2000, in Allen's Astrophysical Quantities, ed. A. N. Cox (New York: Springer) 315
Canup, R. M. 2004, ARA&A, 42, 441
Canup, R. M., & Ward, W. R. 2002, AJ, 124, 3404
Chen, C. H., & Jura, M. 2001, ApJ, 560, L171
Chen, C. H., et al. 2006, ApJS, 166, 351
Debes, J. H., & Sigurdsson, S. 2002, ApJ, 572, 556
Dufour, P., et al. 2007, ApJ, 663, 1291
Dupuis, J., Fontaine, G., Pelletier, C., & Wesemael, F. 1993, ApJS, 84, 73
Farihi, J., Becklin, E. E., & Zuckerman, B. 2008, ApJ, 681, 1470
Farihi, J., Jura, M., & Zuckerman, B. 2009, ApJ, 694, 805
Gaensicke, B. T., Koester, D., Marsh, T. R., Rebassa-Mansergas, A., & Southworth, J. 2008, MNRAS, 391, L103
Gaensicke, B. T., Marsh, T. R., & Southworth, J. 2007, MNRAS, 380, L35
Gaensicke, B. T., Marsh, T. R., Southworth, J., & Rebassa-Mansergas, A. 2006, Science, 314, 1908
Gianninas, A., Dufour, P., & Bergeron, P. 2004, ApJ, 617, L57
Holberg, J. B., Bergeron, P., & Gianninas, A. 2008b, AJ, 135, 1239
Holberg, J. B., Sion, E. M., Oswalt, T., McCook, G. P., Foran, S., & Subasavage, J. P. 2008a, AJ, 135, 1225
Jura, M. 2003, ApJ, 584, L91
Jura, M. 2004, ApJ, 603, 729
Jura, M. 2006, ApJ, 653, 613
Jura, M. 2008, AJ, 135, 1785
Jura, M., Farihi, J., & Zuckerman, B. 2007a, ApJ, 663, 1285
Jura, M., Farihi, J., Zuckerman, B., & Becklin, E. E. 2007b, AJ, 133, 1927
Kilic, M., Farihi, J., Nitta, A., & Leggett, S. K. 2008b, AJ, 136, 111
Kilic, M., Thorstensen, J. R., & Koester, D. 2008a, ApJ, 689, 45
Kilic, M., von Hippel, T., Leggett, S. K., & Winget, D. E. 2005, ApJ, 632, L115
Koester, D. 2009, A&A, 498, 517
Koester, D., Napiwotzki, R., Voss, B., Homeier, D., & Reimers, D. 2005, A&A, 439, 317
Koester, D., & Wilken, D. 2006, A&A, 453, 1051
Kraft, R. P., Burrows, D. N., & Nousek, J. A. 1991, ApJ, 374, 344
Kuijpers, J., & Pringle, J. E. 1982, A&A, 114, L4
Liebert, J., Bergeron, P., & Holberg, J. B. 2005, ApJS, 156, 47
McCord, T. B., & Sotin, C. 2005, J. Geophys. Res., 110, 5009
Michalak, G. 2000, A&A, 360, 363
O'Dwyer, I. J., Chu, Y.-H., Gruendl, R. A., Guerrero, M., & Webbink, R. F. 2003, AJ, 125, 2239
Palme, H., & O'Neill, H. St. C. 2004, in Treatise on Geochemistry, Vol. 2, The Mantle and Core, ed. H. D. Holland & K. K. Turekian, (Amsterdam: Elsevier)
Patterson, J., & Raymond, J. C. 1985, ApJ, 292, 535
Reach, W. T., Kuchner, M., von Hippel, T., Burrows, A., Mullally, F., Kilic, M., & Winget, D. E. 2005, ApJ, 635, 161
Reach, W. T., Lisse, C., von Hippel, T., & Mullally, F. 2009, ApJ, 693, 697
Rhee, J. H., Song, I., & Zuckerman, B. 2008, ApJ, 675, 777
Rieke, G. H., et al. 2004, ApJS, 154, 25
Schmidt, G. D., Szkody, P., Henden, A., Anderson, S. F., Lamb, D. Q., Margon, B., & Schneider, D. P. 2007, ApJ, 654, 521
Song, I., Zuckerman, B., Weinberger, A. J., & Becklin, E. E. 2005, Nature, 436, 363
Struder, L., et al. 2001, A&A, 365, L18
Szkody, P., et al. 2004, AJ, 128, 2443
Thomas, P. C., Parker, J. Wm., McFadden, L. A., Russell, C. T., Stern, S. A., Sykes, M. V., & Young, E. F. 2005, Nature, 437, 224
Tremblay, P.-E., & Bergeron, P. 2008, ApJ, 672, 1144
Turner, M. J. L., et al. 2001, A&A, 365, L27
von Hippel, T., Kuchner, M. J., Kilic, M., Mullaly, F., & Reach, W. T. 2007, ApJ, 662, 544
Voss, B., Koester, D., Napiwotzki, R., Christlieb, N., & Reimers, D. 2007, A&A, 470, 1079
Werner, M. W., et al. 2004, ApJS, 154, 1
Wood, B. J., Pawley, A., & Frost, D. R. 1996, Phil Trans. R. Soc. London A, 354, 1495
Zuckerman, B., & Becklin, E. E. 1987, Nature, 330, 138
Zuckerman, B., Koester, D., Melis, C, Hansen, B. M., & Jura, M. 2007, ApJ, 671, 872
Zuckerman, B., Koester, D., Reid, I. N., & Hunsch, M. 2003, ApJ, 596, 477